MARMARA UNIVERSITY

FACULTY OF ENGINEERING

Redesign of a Centrifugal Casting Machine into a Functional Ball Milling System with Experimental Evaluation

Hüseyin Furkan DEV, Enes TAŞCI, Tarık Buğra USTA

GRADUATION PROJECT REPORT

Department of Mechanical Engineering

Supervisor
Prof. Dr. Aykut Kentli

ISTANBUL, 2025

MARMARA UNIVERSITY

FACULTY OF ENGINEERING

Redesign of a Centrifugal Casting Machine into a Functional Ball Milling System with Experimental Evaluation

by

Hüseyin Furkan DEV, Enes TAŞCI, Tarık Buğra USTA

June 23, 2025, Istanbul

SUBMITTED TO THE DEPARTMENT OF MECHANICAL ENGINEERING IN PARTIAL FULFILLMENT OF THE REQUIREMENTS FOR THE DEGREE

OF

BACHELOR OF SCIENCE

AT

MARMARA UNIVERSITY

Signature of Author(s) .....

Department of Mechanical Engineering

Certified By .....

Project Supervisor, Department of Mechanical Engineering

Accepted By.....

Head of the Department of Mechanical Engineering

ACKNOWLEDGEMENT

First of all, we would like to thank our supervisor Prof. Dr. Aykut Kentli, who guided us during this project. He shared his knowledge and experience and supported us whenever we needed help. His advice was very important for the success of our work.

We are also thankful to our families, who always stood by us and motivated us through this process.

We would like to express our sincere thanks to the workshop technicians who helped us with the practical parts of the project. Their experience and support made it easier for us to complete the mechanical work safely and correctly.

Finally, we would also like to thank the Advanced Manufacturing Processes Laboratory for providing us with access to equipment and technical infrastructure. Their support played a key role in realizing our experimental work.

JUNE, 2025

Hüseyin Furkan DEV

Enes TAŞCI

Tarık Buğra USTA

CONTENTS

ABSTRACT

This project focuses on redesigning an old centrifugal casting machine and converting it into a functional ball milling system. Several mechanical and electrical modifications were made to adapt the existing structure for grinding operations. A custom drum cover was designed and manufactured to ensure safety and containment during rotation. Additionally, the motor wiring was renewed and configured in a star connection for safer and more stable operation. Grinding balls with a diameter of 22 mm were selected, and the system was calibrated to operate at an effective rotational speed.

To evaluate the machine's performance, an experimental study was conducted using three different materials: SD52 steel chips, PLA filament, and aluminum foil. Each material was milled for one hour, with samples collected every 15 minutes. These samples were analyzed under a microscope, and surface area measurements were taken using calibrated imaging software.

The results showed that the milling efficiency varied depending on the material's mechanical properties. Aluminum foil fragmented rapidly but inconsistently, steel chips required longer durations to grind, and PLA demonstrated a stable, progressive breakdown. These findings confirm the machine's capability to grind various material types effectively after the redesign.

SYMBOL

$\sum M_A$: Total Moment of point A

R_B^Z: Reaction force of point B relative to z axis

°: Angle

$\sum M_B$: Total Moment of point B

R_A^Z: Reaction force of point A relative to z axis

N: Newton

$\sum M_A^x$: Total Moment of point A relative to x axis

R_B^x: Reaction force of point B relative to x axis

F_x: Force relative to x axis

F: Force

Sin(): Sinus Function

Cos(): Cosinus Function

R_A^x: Reaction force of point A relative to x axis

R_A:Total Force relative to point A

R_B: Total Force relative to point B

min:Minute

C_{10}: Dynamic load capacity.

a_f: Application factor

F_d: Design radial load

x_d: Desired bearing life

x_0: Weibull parameter

θ: Upper bound constant in the Weibull distribution

R_d: Reliability

a: Load-life exponent

b: Weibull shape parameter

ln(): ln function

L_D: Desired life of the bearing

L_R: Rated life of the bearing

$C_{10,new}$: Required (adjusted) dynamic load capacity

S_0: Safety factor

W_{drum}: Weight of Mold

W_{ball}: Weight of Ball

W_{total}: Total Weight of System

kg: Kilogram

$\frac{m}{s^2}$: Units of Acceleration

W: Symbol of Weight

d_{drum}: Diameter of Drum

d_{pinion}: Diameter of Pinion

mm: Milimetre

Rpm: Revolution/minute

n_{drum}: Revolution for drum

n_{motor}: Revolution for motor

ABBREVIATIONS

CAD: Computer-Aided Design

EDM: Electrical Discharge Machining

RCCB: Residual Current Circuit Breaker

RPM: Revolutions Per Minute

SD37: Structural Steel Grade

Co: Static Load Rating

C: Dynamic Load Rating

UCP: Unit Cast Pillow block

LIST OF FIGURES

LIST OF TABLES

1. INTRODUCTION

The main purpose of this study was to convert a previously existing centrifugal casting machine into a ball milling machine with proper modifications. At first, the motor connections of the machine were removed. For this reason, we bought a suitable three-phase cable for the motor. Since we were going to put balls and materials into the ball milling system, the total weight increased. Because of this extra load, the motor would be forced at certain times. To protect the motor, we used a current protection relay and a phase protection relay.

Also, the drum (heavy rotating part) of the centrifugal casting machine had an open side, so there was a risk that the materials might fall out during rotation. To prevent this, we used a round steel piece and machined it in a lathe so it could fit tightly into the drum. We also opened 6 holes both on the cover and the drum surface. Then, using a thread tap, we created threaded holes so we could insert metric XXX bolts. After choosing the right bolt length, our system was almost ready. Since the machine had not been used for a long time, some parts were rusty. We cleaned them as much as we could with sandpaper. After all the preparations, we started the experimental part.

The goal of the experiment was to observe how much different types of materials are ground in the same time using the ball milling process. While selecting the materials, we specifically wanted to use materials with different structures. In this way, we aimed to understand which type of material is ground better and more efficiently. We also planned to stop the machine at Periodically to learn which time period gives the best results.

In this study, we decided to use SD37 steel chips, aluminum foil, and PLA filament.

The main reason for using SD37 steel chips was to observe how hard and tough metals behave during ball milling. It is also easy to find since it is a common waste from machining processes.

We chose aluminum foil because it has a soft and ductile structure, and we wanted to see how it reacts to impacts. Since it is thin, we were curious to see the grinding effect on a thin material.

Lastly, we used PLA filament because of its brittle and fibrous nature. PLA is also easy to find as scrap and is widely used today due to its environmentally friendly structure.

With these materials, we planned to examine how materials with high strength, ductility, thin structure, and fibrous behavior respond to grinding. We ran the machine for about 1 hour for each material. To observe the effect of time, we stopped the machine every 15 minutes and

took samples. One of our reasons for doing this was because after a certain time, the particles might start sticking together, burning, or behaving differently. Some materials may not show changes early but start to show results after a longer time. We aimed to observe these reactions.

After taking the samples, we used a microscope (we will specify the brand here) to measure them. To scale the measurements under the microscope, we used millimetric paper. We used the ToupView software to take area measurements and capture images. With its custom scale feature, we measured the surface area of the particles. For each material and each stop, we collected 10 samples, aiming to get more accurate results.

We used steel balls to grind the materials. The number of balls was set to fill one-third of the drum volume. The diameter of each ball was 22 mm, which was large enough to make contact with the material, but also small enough to move between the particles.

2. Theoretical Background

Ball Milling

Ball milling is a mechanical process used to reduce the size of solid materials by grinding them into smaller particles. Ball mills consist of a rotating a cylindrical drum that is filled with balls (typically occupying about 35–45% of the drum's volume for optimal grinding efficiency [1]). When the drum rotates by motor, the balls are lifted and dropped onto the material. This action causes both impact and friction, which is breaking the material into smaller pieces.

2.1 Factors Affecting Ball Mill Performance

The efficiency and output of a ball mill are influenced by a wide range of operational and design-related factors. Each parameter affects the grinding behavior of the mill, the size of the material and energy consumption of the machine. Understanding these factors is essential for designing or improving a milling system, especially in our case where a different machine, such as a centrifugal casting system, is redesigned as a ball mill.

1. **Ball Size and Distribution**

The size of the balls is one of the most important factors in the grinding process. Larger balls generate high impact energy and are suitable for breaking larger particles. However, they can leave smaller particles unprocessed. Smaller balls, on the other hand, offer a greater surface area and better contact with the material which is more effective for grinding. A proper mix of ball sizes, known as a graded charge, often yields better results by combining both impact

and abrasion effects. [1]

2. Ball Load (Ball Filling Ratio)

The ball load refers to the volume percentage of the mill that is occupied by the balls. For optimal grinding 35-45% of the drum's volume should be filled with balls. If ball percentage is low the effects of grinding will also be low. If ball percentage is high then the balls interfere with each other and there will be an energy waste.

3. Rotational Speed

The speed at which the drum rotates determines the trajectory of the balls. If the mill turns too slowly, the balls slide or roll without effective grinding. If the speed is too high, centrifugal force causes the balls to remain stuck to the drum wall, halting the grinding action. The ideal operating speed is usually 65–80% of the critical speed, which is the speed at which centrifugal force equals gravitational force. [1] [2].

4. Feed Characteristics

The nature of the material being ground greatly influences performance. This includes:

Feed size: Smaller feed sizes result in more efficient grinding.

Hardness: Harder materials require more energy and larger balls.

Moisture content: Excessive moisture can cause materials to stick to the balls or drum, leading to inefficient grinding. However, in wet grinding, controlled moisture helps transport particles [2].

5. Drum Design and Size

The diameter and length of the drum impact how the balls move inside the mill. A longer drum can hold more material, but it may also reduce energy efficiency if the length-to-diameter ratio becomes too high. Additionally, the liner shape (such as wave liners or step liners) affects the movement of the balls, impacting the grinding behavior and energy distribution [1].

6. Grinding Type (Dry or Wet)

Ball mills may be operated in either dry or wet modes. Wet grinding typically provides better particle dispersion and allows finer particles to be achieved. It also reduces dust and wear on mill components. However, it requires handling of slurry and additional equipment such as pumps or classifiers. Dry grinding is simpler but can lead to dust generation and poor particle separation [1] [3].

7. Milling Time and Loading Rate

Ball mills may be operated in either dry or wet modes. Wet grinding typically provides better

particle dispersion and allows finer particles to be achieved. It also reduces dust and wear on mill components. However, it requires handling of slurry and additional equipment such as pumps or classifiers. Dry grinding is simpler but can lead to dust generation and poor particle separation [1] [3].

8. Temperature and Heat Generation

During extended operation, friction between balls and material can lead to a temperature rise in the mill. This heat may affect material properties, particularly for heat-sensitive materials like polymers or certain chemicals. Therefore, temperature control (through cooling jackets or intermittent operation) may be necessary [3].

9. Material of the Balls

The material from which the balls are made—such as steel, tungsten carbide, zirconia, or ceramic—affects wear rate, contamination level, and grinding behavior. For example, steel balls are commonly used for robust industrial grinding, while ceramic balls are more suitable for clean, contamination-free milling in pharmaceutical or chemical applications.

These factors are interdependent, meaning changes in one parameter can influence others. In the present study, converting a centrifugal casting machine into a ball milling system required careful evaluation of these variables, especially drum speed, weight distribution, and optimal ball loading. Addressing these aspects ensured that the redesigned system could perform efficient and stable grinding operations.

3. Design and Modification Process

3.1 Initial Phase

The system was designed by repurposing a centrifugal casting unit into a ball milling machine. A horizontally mounted drum is rotated via a gear transmission system, where a motor-driven pinion directly engages with a drum gear, ensuring efficient torque transfer. The drum is supported by four wheels, strategically positioned based on force and moment calculations to maintain balance during rotation. A two-piece steel cover, precisely cut using wire EDM, provides secure enclosure and allows for easy material loading. Based on load analysis, UCP 205 bearings were selected to support the shaft. The entire mechanical setup emphasizes durability, safety, and ease of maintenance.

Figure 1 Ball milling system after assembly

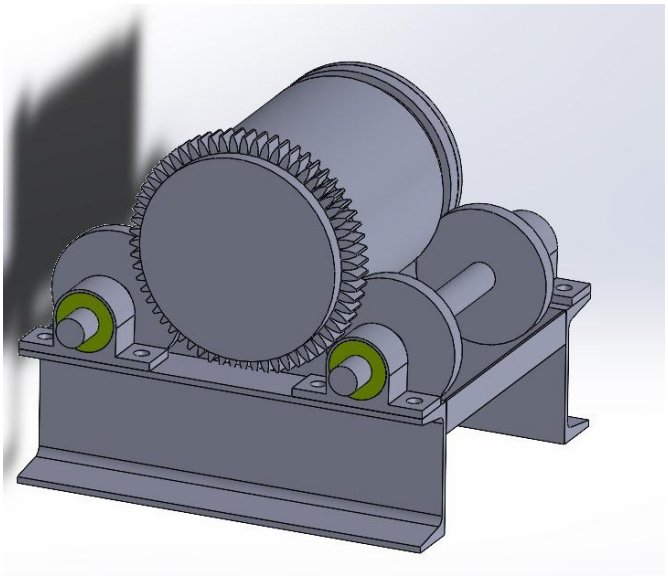

Figure 2 3D CAD representation of the ball milling system

3.2 Design Approach

The primary objective of this project was to convert an idle centrifugal casting machine into a functional ball milling system and to evaluate its grinding performance through experimental trials. However, due to the machine being out of service for a long time, several deficiencies and operational issues were identified. Therefore, the initial phase of the design process focused on a detailed assessment of the machine's current condition and the systematic

elimination of its shortcomings.

The first major issue observed was the absence of electrical connections to the motor. This rendered the machine inoperable and was identified as a priority problem that needed to be resolved in order to enable basic functionality.

The second major deficiency was related to the drum configuration. In centrifugal casting machines, there is no need for a drum cover, resulting in one side of the drum being completely open. In contrast, ball milling systems require the drum to be securely enclosed, as the grinding process involves high-impact collisions between steel balls and the material, which could cause particles to be ejected. For this reason, a mechanically durable and detachable drum cover had to be designed and implemented.

Additionally, due to prolonged disuse, a significant amount of rust and dust accumulation was observed on the outer surfaces of the machine. This not only affected the aesthetic condition of the system but also posed potential operational risks, reducing efficiency and reliability.

While addressing these deficiencies, the entire design process was carefully planned and executed with a focus on ensuring safe, efficient, and cost-effective operation. The following sections of this report detail the corrective steps taken and the technical improvements implemented throughout the redesign process.

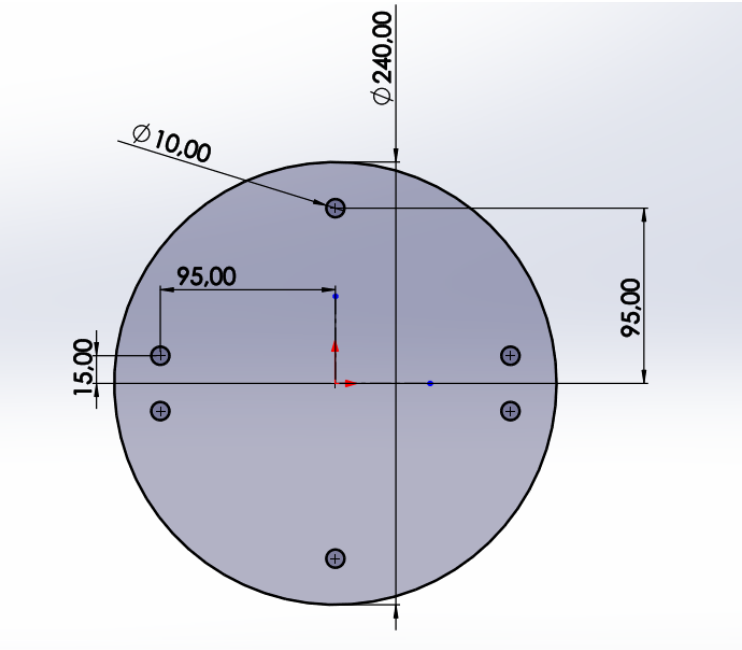

Figure 3 Top view of the drum cover showing the hole layout and key dimensions

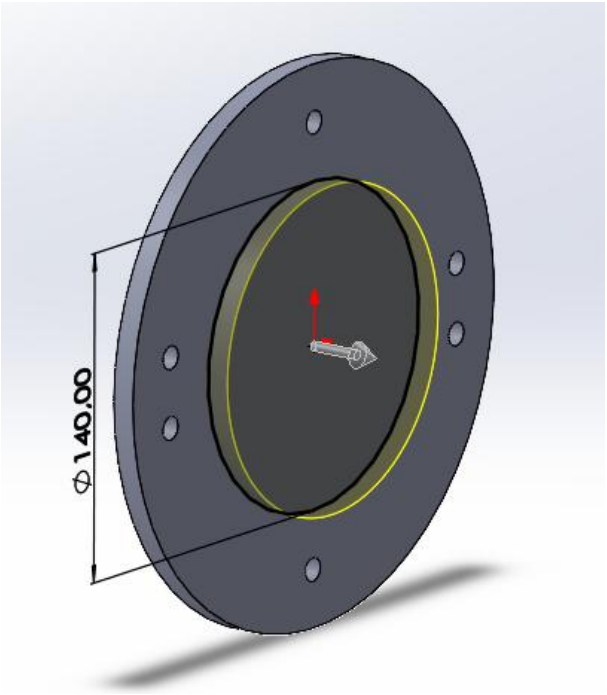

Figure 4 Isometric view of the drum cover with inner recess detail (Ø140 mm).

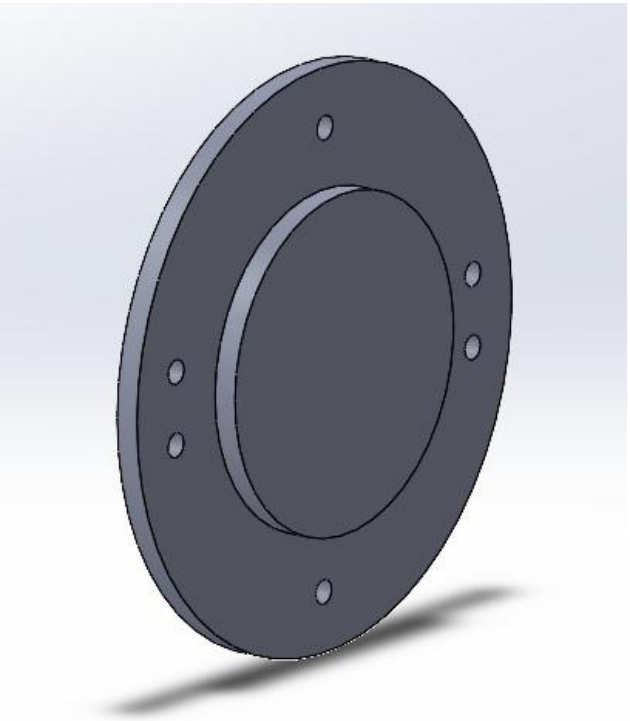

Figure 5 Final CAD model of the two-piece drum cover with bolt holes.

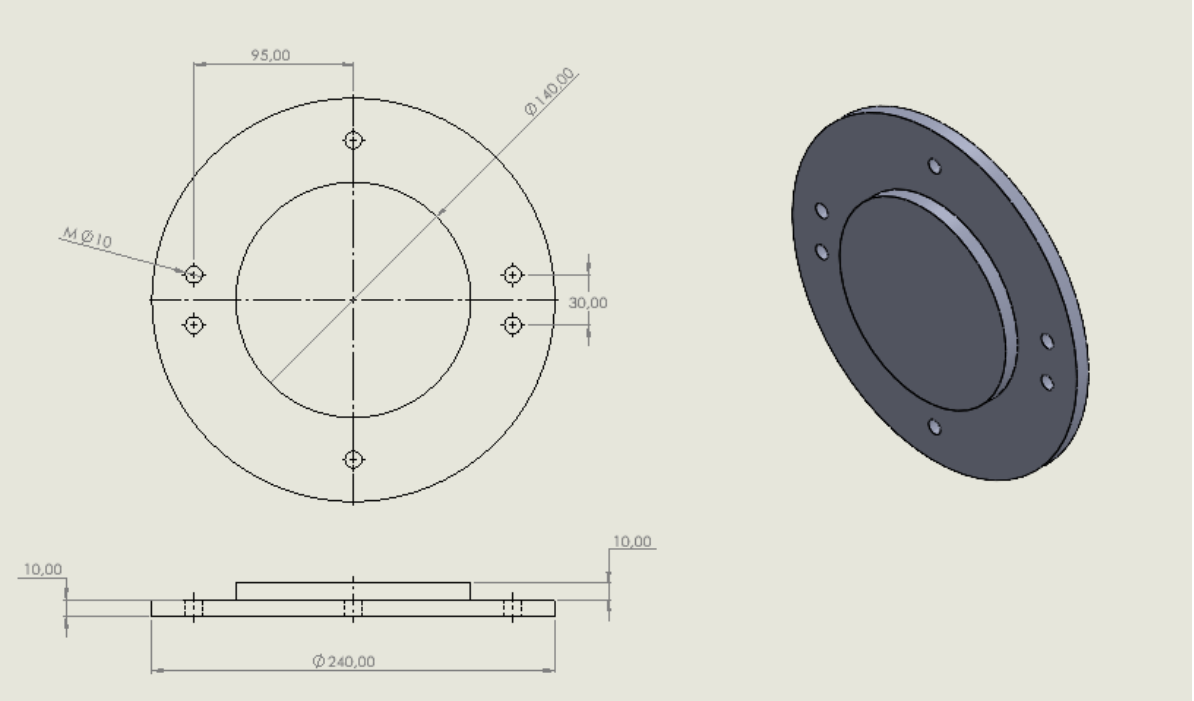

Figure 6 Fully dimensioned technical drawing of the drum cover with front, side, and isometric views.

3.3 Mechanical Modifications

To adapt the centrifugal casting machine into a functional ball milling system, several mechanical modifications were carried out. These modifications focused on ensuring both the safe operation and mechanical suitability of the system. Two primary interventions were performed as part of this process: sealing the drum and removing surface rust.

3.3.1 Drum Sealing and Reinforcement

The drum of the centrifugal casting machine was originally manufactured without a cover, as its previous application did not require one. However, in ball milling operations, high-speed steel balls and materials are continuously agitated, posing a risk of particles being ejected from an open drum. For safety reasons, it was necessary to design and implement a cover that would fit tightly within the inner diameter of the drum and remain clear of any contact with other rotating parts.

To produce such a cover, a suitable steel blank slightly larger than the drum's diameter was first sourced from a scrapyard. This piece was then delivered to a machine shop to be machined to the required inner and outer diameters using a lathe.

The drum cover was designed in two parts to allow for easy removal and material loading.

The lower half was fixed to the drum using M10 bolts, while the upper half allowed insertion of grinding balls and materials into the drum. A total of six threaded bolt holes were tapped into the cover to ensure a robust and secure connection. These threads were carefully created using a tapping tool to allow repeatable fastening.

In order to ensure a perfect fit between the two parts of the cover and prevent leakage or misalignment, the cover piece was split using wire erosion (EDM – Electrical Discharge Machining). This high precision cutting technique provided a smooth and tight joint between the parts.

Each semicircular cover segment was drilled with three symmetrically positioned bolt holes, ensuring mechanical stability and uniform contact pressure across the surface when the bolts were tightened. This configuration resulted in a secure, sealed interface that prevented displacement or vibration during operation.

3.3.2 Rust Removal

Due to prolonged disuse, significant rust formation was observed on the external surfaces, connection points, and gear regions of the centrifugal casting machine. This corrosion was identified as a factor that not only diminished the visual appearance of the machine but also compromised its mechanical functionality and reliability. Therefore, a comprehensive cleaning and rust removal process was carried out.

Initially, the corroded surfaces were mechanically treated using sandpaper to eliminate loose rust and surface contaminants. Following this, chemical rust remover solutions were applied to dissolve remaining oxide layers and to ensure deeper cleaning of the affected areas. Particular attention was given to gear teeth and contact interfaces, which were more susceptible to performance issues such as jamming, loosening, or increased friction due to corrosion.

As a result of these treatments, the overall appearance of the machine was improved, and the functionality of moving components was restored, allowing the system to operate smoothly and without mechanical interference.

3.4 Electrical and Control System Modifications

To enable the ball milling system to operate effectively, all necessary electrical connections and protection circuits were specifically designed and implemented for this project. This section outlines the decisions related to motor connection type, plug compatibility, and control system configuration.

3.4.1 Determination of Connection Type

The electric motor of the centrifugal casting machine did not have any existing wiring in its terminal box. Therefore, the first step was to open the motor's connection box and examine the coil terminals to determine the appropriate wiring configuration. In three-phase asynchronous motors, two common connection types are typically used:

The electric motor of the centrifugal casting machine initially had no wiring in its terminal box. Therefore, the first step in the modification process was to open the motor's connection box and examine the internal coil terminals in order to determine the correct wiring configuration. Three-phase asynchronous motors typically allow for two standard connection methods: star (Y) and delta (Δ) configurations.

In a star (Y) connection, one end of each of the three windings is joined together to form a central neutral point. This configuration is generally preferred in systems that aim to reduce the starting current and minimize voltage drops. In contrast, the delta (Δ) connection links the windings end-to-end, creating a closed loop. This method is typically used in setups that demand higher torque and increased power output.

After evaluating the motor's nameplate data and inspecting the remaining wiring traces, it was concluded that a star connection would be more appropriate for this application. This configuration helps to reduce the inrush current at startup and provides protection against overloading. The required connections were made accordingly, and the motor was successfully wired in a star configuration.

Following this, a compatible industrial-grade three-phase plug was selected based on the socket type available in the university's workshop. The chosen plug met standard electrical safety requirements and ensured proper compatibility with the machine's power system.

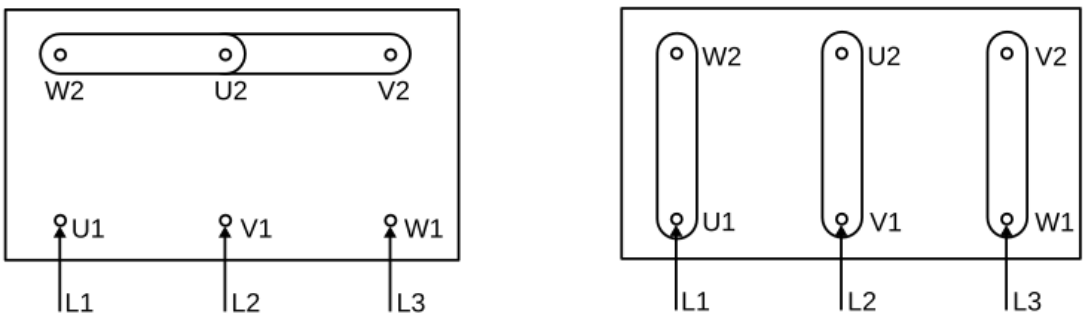

Figure 7 Star (Y) and Delta (Δ) connection diagrams of a three-phase asynchronous motor [4]

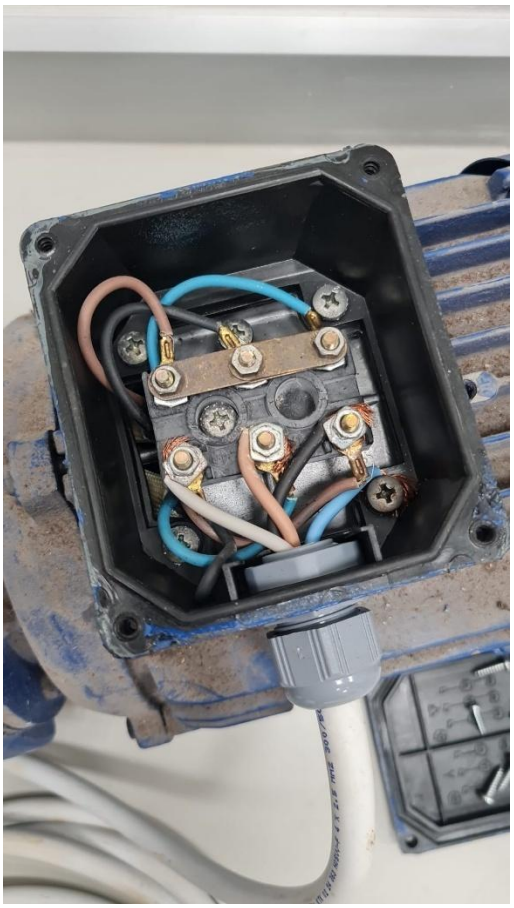

Figure 8 Actual Star (Y) Connection Configuration Used in the Project Motor

3.5 Selection and Arrangement of Grinding Balls

The effectiveness of the grinding process in a ball milling system is strongly influenced by the size, number, and spatial distribution of the grinding balls inside the drum. In this project, 22 mm diameter steel balls were selected as the grinding media. This particular size was chosen because it offers an effective balance between impact force and surface contact. Larger balls can generate greater impact energy, while smaller balls enhance grinding efficiency by increasing surface friction. A 22 mm diameter was found to be an optimal compromise between these two effects.

The selected ball size was also compatible with the internal geometry of the drum. It allowed for free movement of the balls without the risk of jamming, which ensured continuous and smooth circulation during the rotation of the system. Additionally, the chosen diameter was considered suitable for all the materials tested in the experimental studies, including SD37 steel chips, aluminum foil, and PLA filament. These materials have different mechanical

characteristics, and the selected balls provided a sufficient impact profile to effectively grind both hard and soft substances.

Before the grinding process began, the internal volume of the drum was calculated. According to recommendations in the literature, approximately one-third of the total volume should be filled with grinding media for optimal performance. This 33% fill ratio allows for both effective grinding force and adequate space for the balls to move freely. Based on these calculations, 67 steel balls were used to achieve the target volume ratio. This quantity was sufficient to ensure frequent contact between the balls and the material, while avoiding excessive ball-to-ball collisions that could reduce grinding efficiency through energy loss.

Figure 9 Internal view of the drum partially filled with 22 mm steel balls

3.6 Encountered Failures

During the setup and testing phases of the project, several unexpected failures occurred. These issues primarily stemmed from observations related to the electrical components of the system. Throughout the troubleshooting process, various corrective and preventive measures were implemented. This section provides a detailed explanation of the major failure encountered—specifically the motor malfunction—and the solutions developed to address it.

3.6.1 Motor Burnout

Following the completion of the motor's electrical connections, a test run was conducted to verify the operational capability of the system. As the project involved running grinding operations for each material in 15-minute intervals, the same duration was selected for the initial test.

However, the motor stopped suddenly in the 13th minute of the test. This shutdown was triggered by the residual current circuit breaker (RCCB), which activated automatically. Shortly afterward, smoke was observed coming from the motor, indicating potential overheating or a short circuit in the windings. To avoid further damage, the motor was powered down and left to cool.

On the following day, the motor was taken to a certified electric motor repair service for internal inspection. Upon disassembly and examination, it was confirmed that the stator windings were burnt, rendering the motor inoperable and confirming a serious electrical fault.

Causes of Motor Burnout

The root cause of the motor failure was identified as phase imbalance, which resulted in current imbalance across the windings. This imbalance led to an unequal distribution of electrical load, causing excessive current in certain windings and subsequent overheating. During prolonged operation, this overheating degraded the insulation material, ultimately leading to a burnout of the stator coils.

3.7 Load Analysis and Bearing Selection

In order to ensure safe and stable rotation of the drum during the milling process, it was necessary to calculate the total static load acting on the support wheels. This load includes the combined weight of the drum and the grinding media. By analyzing the distribution of forces through the supporting structure, the required load-bearing capacity for each wheel was determined. The calculations were carried out by resolving the vertical force into symmetrical components, considering the angular placement of the wheels and the total system weight.

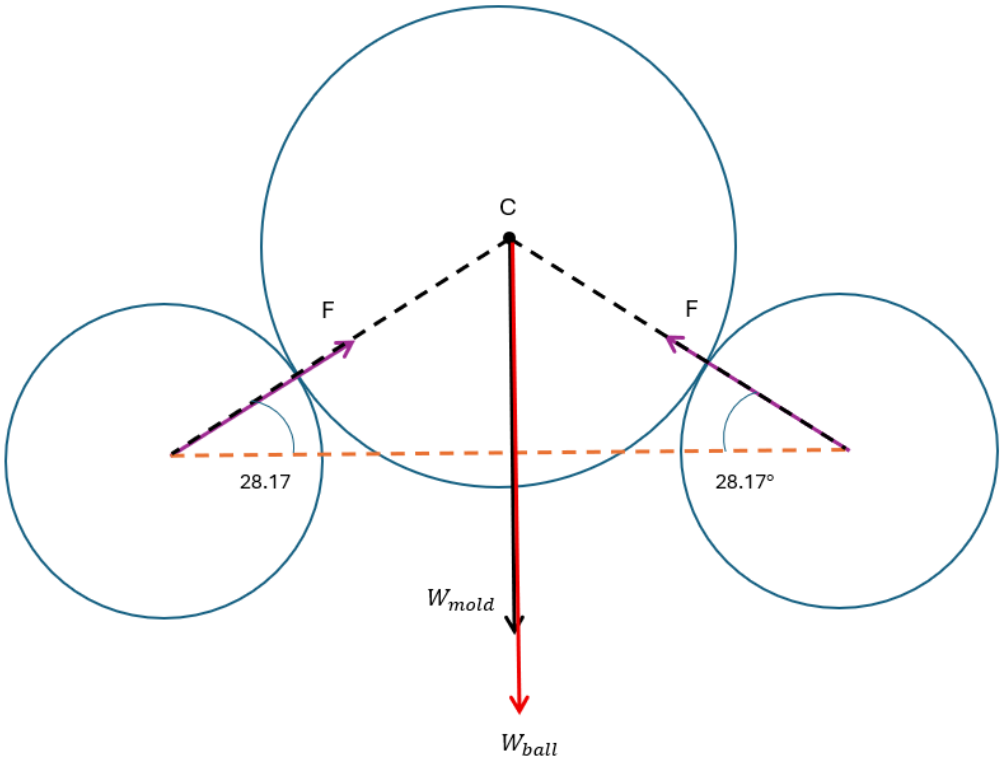

Figure 10 Free-body diagram showing the vertical weight and its symmetrical distribution on support wheels

$$W_{mold} = 735.75\ N \tag{1}$$

$$W_{ball} = 67 * (0{,}0436kg) * \left(9.81 \frac{m}{s^2}\right) = 28.65\ N \tag{2}$$

$$W_{total} = W_{ball} + W_{mold} = 735.75 + 28.65 = 764.4\ N \tag{3}$$

Number of Wheels = 4;

$$4 * F * \sin(28.17°) = W \tag{4}$$

$$F = \frac{764.4}{4 * \sin(28.17°)} \tag{5}$$

$$F = 404.8\ N \tag{6}$$

These calculations were performed to determine the total vertical load acting on the system and the corresponding support force required from each of the four wheels or bearings. The total weight includes the mass of the drum and the grinding media (steel balls), which together create a downward force on the support structure. Considering the angular arrangement of the wheels at 28.17°, the vertical load was decomposed into force components using trigonometric relationships. The resulting reaction force indicates the minimum load capacity

each support point must withstand to ensure mechanical stability during operation.

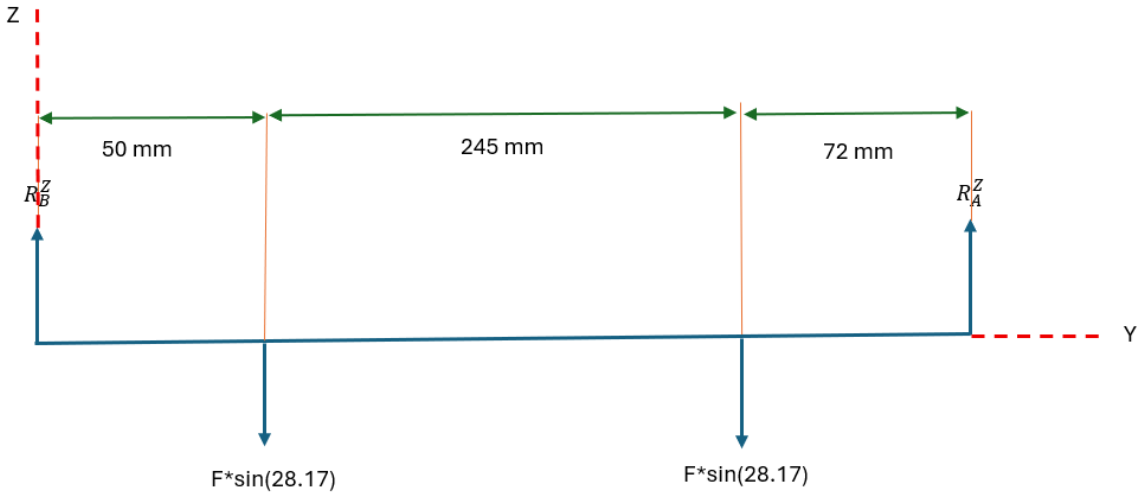

Figure 11 Force distribution and reaction calculation diagram for the support shaft

$$\sum M_A = 0 \tag{7}$$

$$R_B^Z \cdot 367 = \mathrm{F} \cdot \sin(28.17°) \cdot (317 + 72) \tag{8}$$

$$R_B^Z = \frac{404.8 \cdot \sin(28.17°) \cdot 389}{367} \tag{9}$$

$$R_B^Z = 202.55\,\mathrm{N} \tag{10}$$

$$\sum M_B = 0 \tag{11}$$

$$R_A^Z \cdot 367 = F \cdot \sin(28.17°) \cdot (50 + 295) \tag{12}$$

$$R_A^Z = \frac{404.8 \cdot \sin(28.17°) \cdot 345}{367} \tag{13}$$

$$R_A^Z = 179.64\,N \tag{14}$$

To determine the reaction forces acting on the shaft supports, a static moment balance analysis was performed. The system was considered in equilibrium, and moment equations were written with respect to each support point. By summing the moments about point A and point B separately, the vertical reaction forces R_B^Z and R_A^Z were calculated. These reactions represent the loads transferred to the shaft support bearings, considering the eccentric position of the applied forces. The known geometry of the shaft and the calculated vertical forces F·sin(28.17°) were used in the moment equations. As a result, the bearings were found to carry approximately 202.55 N and 179.64 N, respectively, ensuring proper load distribution

across the support structure.

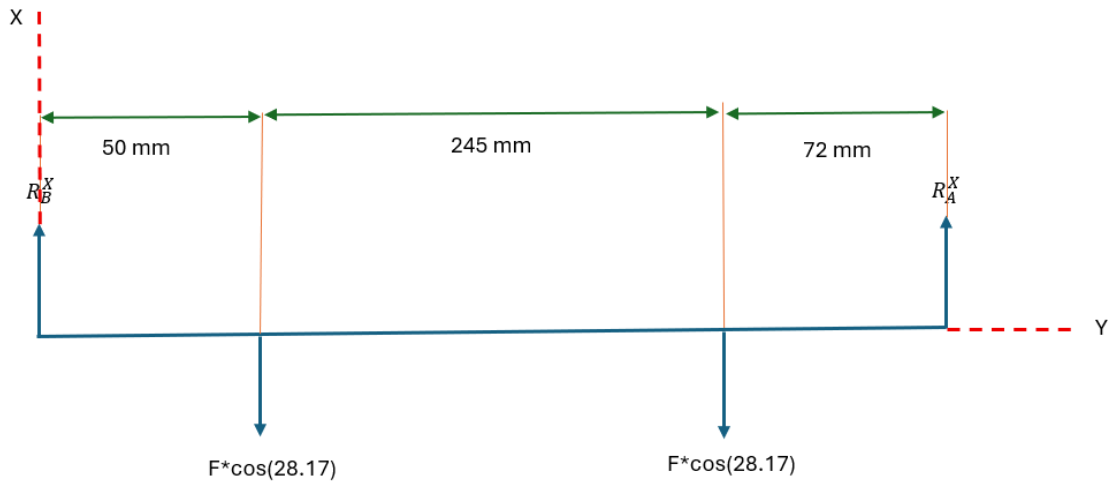

Figure 12 Free-body diagram showing the horizontal force components acting on the shaft

$$\sum M_A^x = 0 \tag{15}$$

$$R_B^x \cdot 367 = F_x \cdot \cos(28.17°) \cdot (317 + 72) \tag{16}$$

$$R_B^x = \frac{404.8 \cdot \cos(28.17°) \cdot 389}{367} \tag{17}$$

$$R_B^x = 378.24\,\text{N} \tag{18}$$

$$\sum M_B^x = 0 \tag{19}$$

$$R_A^x \cdot 367 = F_x \cdot \cos(28.17°) \cdot (50 + 295) \tag{20}$$

$$R_A^x = \frac{404.8 \cdot \cos(28.17°) \cdot 345}{367} \tag{21}$$

$$R_A^x = 335.46\,\text{N} \tag{22}$$

Resultant Force

$$R_A = \sqrt{(R_A^x)^2 + (R_A^Z)^2} \tag{23}$$

$$R_A = \sqrt{(335.46)^2 + (179.64)^2} \tag{24}$$

$$R_A = 380.53\,\text{N} \tag{25}$$

$$R_B = \sqrt{(R_B^x)^2 + (R_B^Z)^2} \tag{26}$$

$$R_B = \sqrt{(378.24)^2 + (202.55)^2} \tag{27}$$

$$R_B = 429.05\,\text{N} \tag{28}$$

So, the critical point is B and we will make calculations about bearing which located on this point.

A cylindrical roller bearing is subjected to a radial load of 0.429 kN radial load. The life is to be 30000 h. Exhibit a reliability of 0,90.

$$C_{10} = a_f F_D \left\{ \frac{x_D}{x_0 + (\theta - x_0)\left[\ln\left(\frac{1}{R_D}\right)\right]^{\frac{1}{b}}} \right\}^{\frac{1}{a}} \tag{29}$$

Using the Weibull parameters as x_0=0.02, (θ-x_0)=4.439 and b=1.483, when R_D=0.90, the expression in the denominator of the above equation reduces to

$$x_0 + (\theta - x_0)\left[\ln\left(\frac{1}{R_D}\right)\right]^{\frac{1}{b}} \tag{30}$$

$$= 0.02 + 4.439\left[\ln\left(\frac{1}{0.90}\right)\right]^{\frac{1}{1.483}} = 0.99 \approx 1 \tag{31}$$

$$C_{10} = a_f * F_D \cdot x_D^{\frac{1}{a}} \tag{32}$$

$$a = 10/3\ for\ cylindical\ roller\ bearing \tag{33}$$

$$x_D = \frac{L_D}{L_R} = \frac{60 * \mathcal{L}_D * n_D}{L_R} \tag{34}$$

$$L_R = 10^6, L_D = 30000h * 60min/h * 800rev/min = 1{,}440{,}000{,}000\ rev\# \tag{35}$$

$$x_D = \frac{L_D}{L_R} = \frac{1{,}440{,}000{,}000\ rev}{10^6} = 1440 \tag{36}$$

$$C_{10} = a_f * F_D * x_D^{1/a} = 1{,}2 * 429N * (1440)^{\frac{3}{10}} = 4562{,}54\ N \tag{37}$$

$$C_{10} * 2 = 9125{,}09\ N \tag{38}$$

Since there are 2 F forces at points a and b, we multiply C_{10} by 2. If we take the safety factor as 1 in this design, the c10 value of our bearing will be:

$$C_{10} = 9125{,}09\ N \tag{39}$$

$$C_{10,new} \geq S_0 \cdot C_{10} \tag{40}$$

$$C_{10,new} \geq 1.5\ *\ 9125{,}09\ \text{N} \tag{41}$$

$$C_{10,new} \geq 13687{,}63\ N \tag{42}$$

The suitable bearing was selected for us from the bearing catalogue.

Table 1 Technical specifications of UCP 205 series bearing units [5]

RULMAN NO	BOYUTLAR (mm)											Yük Sayısı (KN)		Devir-Hız Sınırı (devir/dak.)	Cıvata Ölçüsü	Ağırlık (kg)
	d	H	L	J	A	N	N1	H1	Ho	B	S	Dinamik (C)	Statik (Co)			
UCP 201	12	30,2	127	95	38	13	19	14	61	31	12,7	12,82	6,65	4000	M10	0,7
UCP 202	15	30,2	127	95	38	13	19	14	61	31	12,7	12,82	6,65	4000	M10	0,72
UCP 203	17	30,2	127	95	38	13	19	14	61	31	12,7	12,82	6,65	4000	M10	0,74
UCP 204	20	33,3	127	95	38	13	19	14	64	31	12,7	12,82	6,65	4000	M10	0,76
UCP 205	25	36,5	140	105	38	13	19	15	71	34,1	14,3	14,03	8,05	3400	M10	0,76
UCP 206	30	42,9	160	121	44	17	21	16	82	38,1	15,9	19,47	11,43	2800	M14	1,25
UCP 207	35	47,6	167	126	48	17	21	17	92	42,9	17,5	25,69	15,55	2400	M14	1,55

Figure 13 UCP series pillow block bearing unit used in the system [5]

Although the dynamic load capacity of the selected bearing (UCP 205) is specified as 14.03 kN, the total calculated load acting on the system was approximately 13.687 kN. Since this value is very close to the bearing's limit, we intentionally avoided filling the drum with grinding balls up to the commonly used 30% of total volume. This decision was made to prevent overstressing the bearing and to ensure long-term operational safety and mechanical integrity of the machine.

3.8 Drum Rotational Speed Calculation

In order to determine the rotational speed of the drum, the gear ratio between the pinion and drum was taken into account. The output speed of the electric motor was measured as 556 rpm. Using the ratio of the pinion diameter (140 mm) to the drum diameter (220 mm), the drum speed was calculated with the classical gear reduction formula. As a result, the drum was found to rotate at approximately 353.81 rpm under operating conditions.

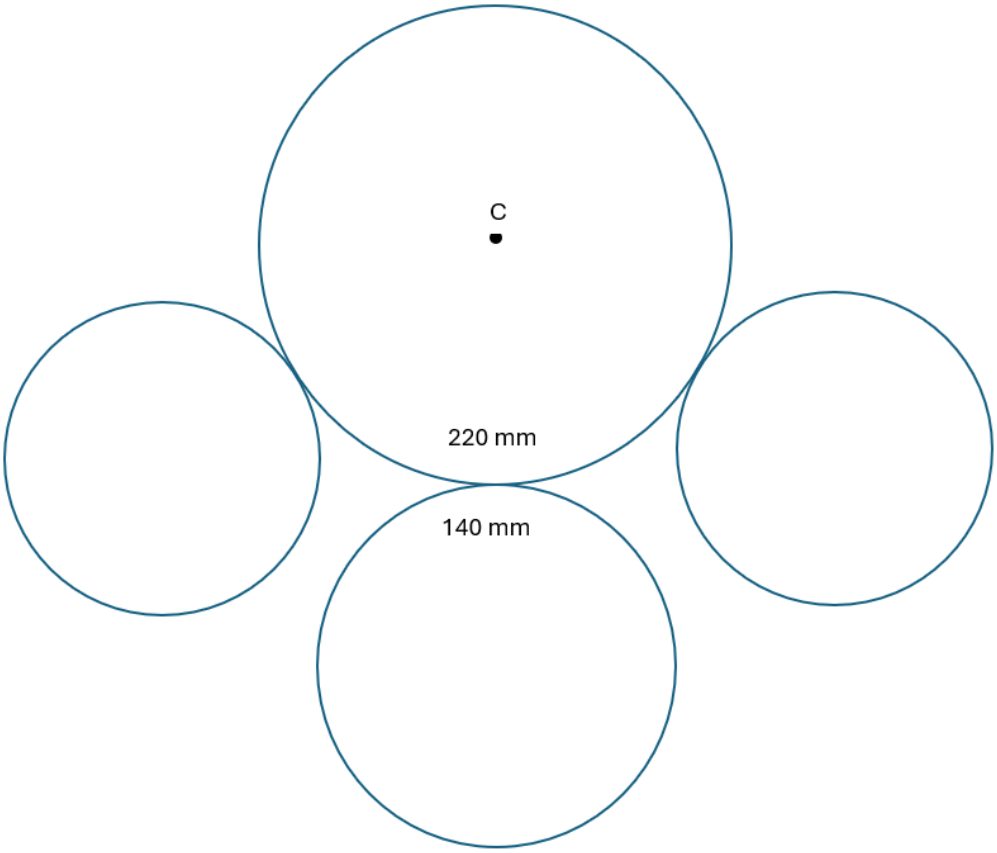

Figure 14 Schematic representation of the drum and driving roller configuration

$$d_{drum} = 220\ mm\ , d_{pinion} = 140mm \tag{43}$$

The output speed of our engine = 556 rpm, we calculate drum's rpm:

$$n_{drum} = n_{\text{motor}} \times \frac{d_{\text{pinion}}}{d_{\text{drum}}} = 556 \times \frac{140}{220} = 353.81rpm \tag{44}$$

4. Experimental Study

4.1 Experimental Procedure

To begin the experiment, three types of materials—PLA filament, aluminum foil, and DS52

steel chips—were selected due to their different mechanical properties. PLA is a brittle and fibrous thermoplastic, aluminum is a soft and ductile metal, and DS52 is a strong and hard steel alloy. These differences made it possible to compare how various types of materials respond to the same milling process under the same conditions.

Before starting the milling process, we took a set of 10 individual pieces from each material. These initial samples were used as a reference to evaluate how much grinding occurred after each time period. The particles were placed under a microscope and measured using the ToupView software. In order to scale the images correctly, millimetric graph paper was used as a background. The average surface area of these 10 samples was recorded as the "starting size" for each material.

After initial measurements were completed, the ball milling machine was prepared for operation. Each material was placed into the drum individually, and the machine was run for 60 minutes per material. During this one-hour operation, the machine was paused at 15-minute intervals. At each of these intervals (15, 30, 45, and 60 minutes), 10 samples were taken from the material inside the drum.

These samples were again analyzed under the microscope. Their images were captured using the same scaling method with millimetric paper, and surface area values were calculated using ToupView. This approach ensured consistency in the measurement technique and reduced the chance of human error.

By taking 10 samples per interval and calculating their average surface areas, we aimed to track the changes in particle size more reliably. The use of multiple samples also helped minimize the effect of irregularly shaped particles or outliers.

One important reason for choosing a 15-minute interval was to observe whether certain materials would show early signs of grinding or whether they would need a longer exposure time. In some cases, particles may not change significantly at the beginning, but may become more affected as the machine continues to run. On the other hand, softer materials might start clumping together or breaking down very quickly. For this reason, regular observation was essential.

To maintain fair testing conditions, the same number of steel balls and the same drum fill level were used for each experiment. The balls were 22 mm in diameter and filled one-third of the drum volume. No additional lubrication or cooling was applied during milling, to keep all tests under identical dry conditions.

This experimental method allowed us to collect data at consistent time intervals and under

stable conditions. As a result, we were able to compare the grinding efficiency of different materials and better understand their behavior in a ball milling system.

4.2 Measurement Tools and Analysis Method

To analyze the surface areas of the milled particles, a Nikon SMZ 745T stereo microscope was used. This microscope provides clear, zoomed-in images of small objects and is suitable for observing materials with different shapes and surface structures. The microscope was connected to a computer, allowing us to capture images of the samples for further analysis.

During the measurement process, a piece of millimetric graph paper was placed under the samples. This paper helped us scale the images accurately, so that we could calculate the surface area of each particle. After capturing the images, we used a software called ToupView to analyze them.

ToupView has a feature that allows users to set a custom scale. Using the known dimensions of the millimetric paper as a reference, we calibrated the images in the software. Then, the outlines of the particles were traced using the software's area measurement tool. The program calculated the surface area for each sample based on this calibration.

For each time interval in the experiment (0, 15, 30, 45, and 60 minutes), 10 samples were analyzed. This gave us more accurate average values and helped reduce the impact of any measurement errors. The same microscope, lighting, and scaling method were used for all samples to ensure consistency in the results.

The combination of the Nikon SMZ 745T microscope and ToupView software allowed us to measure and compare the size reduction of the materials in a reliable and repeatable way.

Figure 15 Nikon SMZ745T stereo microscope used for surface area measurements during particle size analysis.

5. Results and Discussion

5.1 Overview of Experimental Results

The ball milling experiments conducted on PLA filament, aluminum foil, and DS52 steel chips provided clear differences in grinding behavior over time. Even though the same milling conditions and time intervals were used for all three materials, the change in average surface area varied significantly between them.

The table below shows the average surface area values (in arbitrary units) calculated from 10 samples per time interval for each material:

Table 2 Average Surface Area Values of Materials at Different Milling Times

MATERIAL	0 MIN	15 MIN	30 MIN	45 MIN	60 MIN
ALUMINUM FOIL	5,8 cm^2	1,46 cm^2	60,62 mm^2	0,11 mm^2	0,041 mm^2
PLA FILAMENT	168,338 mm^2	158,37 mm^2	121,98 mm^2	110,13 mm^2	71,075 mm^2

STEEL CHIPS	16,79 mm^2	15,51 mm^2	15,002 mm^2	9,83 mm^2	5,44 mm^2

Note: Each value represents the average surface area of 10 individual samples measured using ToupView software, with millimetric paper as a reference scale.

The results obtained from the ball milling experiments revealed distinct grinding behaviors for each material. Although all tests were conducted under identical conditions, the surface area reduction patterns varied depending on the mechanical properties of the materials.

Steel chips exhibited a gradual yet consistent decrease in average surface area throughout the experiment. The most significant reduction occurred between 30 and 60 minutes, indicating that this material, due to its high hardness and density, requires a longer milling duration to undergo substantial fragmentation. The trend suggests that steel particles resist early deformation but eventually yield to prolonged mechanical impact.

In the case of PLA filament, an unexpected increase in surface area was observed during the first 15 minutes. This may be attributed to the material's fibrous and brittle nature, which could have caused it to break into irregular, thin fragments, initially increasing the total exposed surface. However, after this point, the average surface area began to decrease in a more controlled and continuous manner. This behavior suggests a progressive and predictable grinding pattern compared to the other materials.

Aluminum foil, on the other hand, responded rapidly to the milling process. A sharp decrease in surface area was recorded within the first 15 minutes, consistent with its soft and ductile structure. However, at the 30-minute mark, a sudden spike was detected, likely due to the folding of thin foil particles or inconsistencies in the sample shape during measurement. Despite this anomaly, the overall trend clearly shows that aluminum reached a fine, fragmented state much faster than the other materials.

These observations highlight the strong influence of material properties such as hardness, ductility, and brittleness on the grinding performance in ball milling. Softer and thinner materials like aluminum tend to break down quickly but may produce irregular particle shapes. Tougher materials like steel require extended operation time for effective size reduction, while PLA filament demonstrated a more balanced and progressive fragmentation profile.

5.2 Steel Chips

The grinding behavior of DS52 steel chips revealed a relatively slow but stable trend in size reduction throughout the milling process. According to the measurements, the average surface

area of the particles was 16.79 mm² at the beginning (0 min) and gradually decreased to 15.51 mm² at 15 minutes and 15 mm² at 30 minutes. Although the change in the first 30 minutes was minimal, it still indicated the start of particle wear due to repeated impacts inside the drum.

A more noticeable reduction occurred after 30 minutes, as the average area dropped to 9.83 mm² at 45 minutes and further declined to 5.44 mm² at the 60-minute mark. This late-stage change suggests that the cumulative mechanical stress started to overcome the material's hardness and resistance, leading to fragmentation in the latter half of the experiment.

Steel, being a dense and tough material, typically requires extended periods of milling to break down significantly. The data obtained from this study confirms this behavior. Unlike softer materials, steel chips resist deformation and therefore respond more slowly to grinding forces. However, the final measurement at 60 minutes shows that, with enough time, substantial reduction is possible even for harder materials.

In conclusion, steel chips showed a time-dependent reduction trend, with the most effective grinding occurring after the halfway point of the process. This highlights the importance of extended duration when milling rigid, high-strength materials.

Table 3 Surface Area Measurements of Steel Chips at Different Milling Times

Steel Chips					
Minutes / Sample	0	15	30	45	60
1	29,24	16,18	11,44	5,15	11,73
2	15,46	25,12	18,74	10,14	3,52
3	17,42	25,05	15,42	11,03	4,49
4	13,83	10,66	25,16	17,01	5,39
5	7,2	20,5	9,14	4,33	5,83
6	17,96	8,02	13,06	10,36	0,86
7	17,77	11,14	13,07	12,01	1,02
8	15,6	6,74	13,4	12,89	2,49
9	16,68	18,91	10,47	9,56	13,4

10	16,79	12,83	20,12	5,86	5,74
AVERAGE	16,795	15,515	15,002	9,834	5,447
UNIT	mm^2	mm^2	mm^2	mm^2	mm^2

Figure 16 Visual comparison of steel chip samples after different milling durations (0, 15, 30, and 45 minutes), showing the progressive reduction in particle size and shape deformation over time.

5.3 PLA Filament

The grinding behavior of PLA (polylactic acid) filament during the ball milling process displayed a more complex and somewhat unexpected pattern compared to the other materials.

At the beginning of the experiment, the average surface area of the PLA particles was measured at 168.34 mm², which was the highest among all three materials tested.

Surprisingly, after 15 minutes of milling, the average surface area decreased only slightly to 158.37 mm², and a more significant drop occurred at 30 minutes, with a value of 121.98 mm². Although this trend suggests that the material was breaking down over time, the initial decrease was slower than expected. One possible explanation is that PLA, being a fibrous and brittle polymer, initially fragmented into thinner strands or irregular shapes, which may have temporarily increased the exposed surface area or affected the uniformity of the samples.

As the milling continued, the surface area continued to decrease gradually. At 45 minutes, it dropped to 110.13 mm², and by the end of the experiment (60 minutes), it reached 71.075 mm². This steady and progressive decline shows that PLA underwent a controlled size reduction throughout the entire milling process.

Compared to aluminum foil and steel chips, PLA filament showed a more balanced and predictable behavior. It did not exhibit sudden jumps or irregular measurements, and the reduction in surface area followed a smoother curve. This behavior is likely related to the nature of PLA, which is known to fracture rather than deform, producing finer and more regular fragments over time.

In summary, PLA filament demonstrated a stable milling response, with a gradual reduction in particle size. While it did not disintegrate as rapidly as aluminum foil, it showed more consistent results than steel chips. These characteristics make PLA a suitable material for applications requiring controlled fragmentation under dry milling conditions.

Table 4 Surface Area Measurements of PLA Filament at Different Milling Times

PLA Filament					
Minutes / Sample	0	15	30	45	60
1	110,76	267,93	145,98	82.61	60,76
2	86,32	156,41	76,19	64,72	42,04
3	129,48	122,34	104,33	121,09	27,22
4	260,53	132,75	85,47	62,29	55,05
5	69,61	126,87	69,02	80,27	58,75

6	462,14	157,22	139,02	70,86	64,63
7	139,95	134,78	125,33	213,07	151,77
8	129,56	136,15	139,15	139,17	60,84
9	92,61	190,93	205,44	138,07	125,06
10	202,42	155,68	129,91	101,65	64,63
AVERAGE	168,338	158,3755556	121,984	110,1322222	71,075
UNIT	mm^2	mm^2	mm^2	mm^2	mm^2

Note: Each value represents the surface area of a single steel chip measured using ToupView software with millimetric scaling. Averages were calculated from 10 samples per time point.

5.4 Aluminum Foil

According to the results presented in the summary table, aluminum foil exhibited the most dramatic and rapid surface area reduction among the three materials tested. At the start of the milling process, the average surface area was measured as 5.8 cm^2, which was already significantly lower than the other materials due to aluminum foil's thin and flexible nature.

After just 15 minutes of milling, the surface area sharply dropped to 1.46 cm^2, demonstrating that aluminum responded almost immediately to the mechanical impacts of the steel balls. This fast breakdown is consistent with the material's soft and ductile characteristics, which make it highly susceptible to tearing and deformation under pressure.

However, an unexpected increase in surface area was recorded at the 30-minute mark, reaching 60.62 mm^2. This sudden spike may be the result of thin foil particles folding over themselves or becoming crumpled, which could increase the projected surface area when viewed under the microscope. Another possibility is overlapping fragments during the sampling process, which might have caused measurement inaccuracies.

Following this irregularity, the milling process continued to reduce the particle size significantly. By 45 minutes, the average surface area had fallen to 0.11 mm^2, and at the end of 60 minutes, it further decreased to 0.041 mm^2. These final values indicate that aluminum foil was eventually transformed into extremely fine fragments, possibly close to powder form.

Overall, aluminum foil demonstrated the fastest milling response, but also showed some instability in measurement due to its physical behavior. The results confirm that while aluminum can be efficiently broken down in a short time, its tendency to bend, fold, and stick

together can introduce fluctuations in surface area data, which must be considered during analysis.

Table 5 Surface Area Measurements of Aluminum Foil at Different Milling Times

Aluminum foil					
Minutes / Sample	0	15	30	45	60
1	4,86	1,59	69,08	0,22	0,01
2	6,8	1,32	82,47	0,03	0,02
3	6,94	1,41	44,45	0,03	0,19
4	6,05	1,06	82,1	0,05	0,06
5	7,2	1,42	60,19	0,21	0,01
6	4,85	1,15	52,5	0,27	0,01
7	5,14	1,46	45,63	0,07	0,02
8	4,35	2,08	69,07	0,15	0,03
9	6,07	2,1	39,13	0,11	0,08
10	6,47	1,07	61,67	0,08	0,01
11	5,1	1,52	58,7	0,06	0,02
AVERAGE	5,802727273	1,466	60,629	0,116363636	0,041818182
UNIT	cm^2	cm^2	mm^2	mm^2	mm^2

Note: Each value is the average of 10 aluminum foil samples per time interval, measured using ToupView software. All measurements were calibrated with millimetric paper.

Figure 17 Representative samples of aluminum foil, PLA filament, and steel chips at various milling intervals (0, 15, 30, and 45 minutes), illustrating the progressive fragmentation and surface morphology changes due to ball milling.

5.5 Comparative Evaluation

In this section, the grinding performance of three distinct materials—aluminum foil, PLA filament, and steel chips is comparatively evaluated based on the reduction in surface area over time during the ball milling process. The surface area measurements, collected at 15-minute intervals over a total duration of 60 minutes, have been normalized to express the remaining surface area of each sample as a percentage of its original size at 0 minutes. This normalization allows for a clearer, dimensionless comparison of grinding behavior across materials with vastly different initial sizes and physical characteristics.

To better illustrate the trend and compare the efficiency of the milling process, Table 6

presents the calculated percentage of surface area remaining at each time interval for all three materials. This table provides a direct numerical comparison of how the surface areas evolved during the grinding process. In addition, Figure 14 visualizes these trends, showing the percentage-based change in surface area on a time axis, enabling a straightforward graphical interpretation of milling efficiency.

Table 6 Percentage of Remaining Surface Area of Materials at Different Milling Times

Milling Time (min)	Aluminum Foil (%)	PLA Filament (%)	Steel Chips (%)
0	100.00	100.00	100.00
15	25.28	94.08	92.38
30	10.45	72.46	89.35
45	0.02	65.42	58.57
60	0.007	42.22	32.44

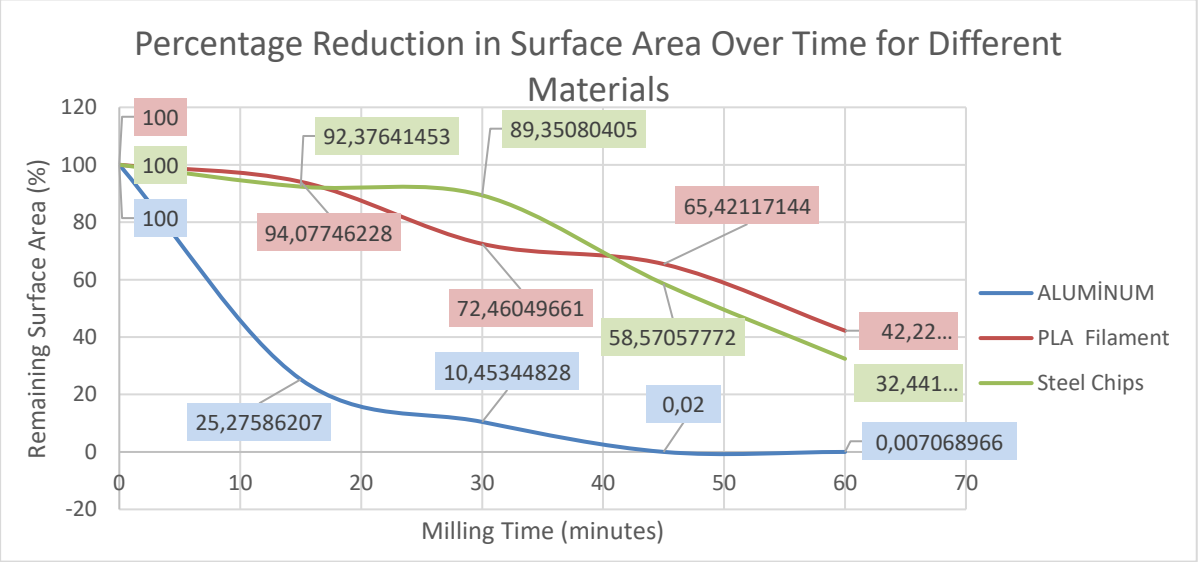

Figure 18 Percentage Reduction in Surface Area Over Time for Different Materials

As seen in both the table and the graph, aluminum foil exhibited the most rapid degradation, showing an extremely steep decline in surface area within the first 15 minutes of milling. With over 74% of its surface area eliminated in just 15 minutes, and more than 99.9% removed by the 45-minute mark, aluminum clearly demonstrated the highest grinding efficiency under the given conditions. This can be attributed to its high ductility and low hardness, which allow the material to be quickly deformed, crumpled, and fragmented under the impact of the steel balls. Moreover, its thin and malleable sheet-like structure further facilitates tearing and

folding during milling, accelerating surface reduction.

In contrast, PLA filament displayed a significantly slower and smoother reduction trend. By the 30-minute mark, only 27.5% of the surface area was lost, and even after 60 minutes, over 42% of the original surface remained intact. The relatively gradual decline observed here is a result of the material's fibrous and brittle polymeric structure, which does not lend itself to rapid pulverization. Instead, the filament tends to shred into elongated strands rather than instantly break down into fine particles. This behavior results in a higher residual surface area throughout the process. PLA's polymer chains may also provide mechanical resistance to compression and shear forces, slowing the milling rate despite continuous exposure.

Meanwhile, steel chips demonstrated a hybrid response between the two extremes. In the first 30 minutes, the material showed only minimal surface loss (approximately 10%), indicative of its high strength, hardness, and toughness. However, beyond the 30-minute mark, the breakdown process became more significant. By the end of 60 minutes, approximately 67.6% of the original surface area had been ground away. This delayed response reflects the energy-intensive nature of grinding metallic materials like steel. Unlike aluminum, steel does not deform easily under impact; instead, it requires repeated high-energy collisions to initiate cracking and chipping. Once initial micro-fractures propagate through the chip structure, the reduction in size accelerates due to accumulated fatigue and fragmentation.

From a comparative performance perspective, it is evident that aluminum foil was the material most rapidly broken down during the milling process. It reached near-total pulverization even before half of the total milling duration had passed, due to its soft, ductile structure and thin geometry, which allowed for quick tearing and crumpling. In contrast, PLA filament resisted rapid surface reduction but gradually degraded over time, demonstrating a smoother and more consistent grinding profile. This behavior can be attributed to its fibrous, brittle nature, which leads to slower fragmentation. Steel chips, while showing strong resistance at the beginning, started to break down more noticeably after extended milling. Their tough and hard structure required longer exposure to impact forces, but eventually responded, indicating that steel is better suited for longer-duration grinding when fine particle sizes are desired.

These findings highlight the influence of material properties—such as hardness, ductility, toughness, and geometry—on grinding behavior. The results emphasize that optimal milling time and ball-to-powder ratios must be carefully tailored depending on the target material's characteristics. A one-size-fits-all milling schedule is not suitable when dealing with heterogeneous materials, especially those combining metals and polymers.

In conclusion, the percentage-based evaluation of surface area reduction provides a powerful framework for assessing the effectiveness of the grinding process across different materials. The plotted graph and numerical data serve as valuable indicators for optimizing milling parameters and tailoring equipment settings to match material-specific requirements in future designs and experiments.

5.6 Discussion

The experimental results of this study provide valuable insight into how different material types respond to ball milling under identical operational conditions. The analysis clearly indicates that the milling performance is highly dependent on the intrinsic physical properties of each material—such as hardness, toughness, ductility, and geometry—which influence the material's resistance to fragmentation under repeated impact.

Aluminum foil showed the most rapid reduction in surface area, reaching near-total pulverization within the first 45 minutes of the process. This exceptional milling performance is mainly attributed to aluminum's low hardness, high ductility, and extremely thin sheet-like structure. These characteristics enable the material to deform, fold, and tear easily under the impact of steel balls, leading to fast surface reduction. The steep curve seen in the data and the resulting minimal residual area demonstrate that aluminum foil is highly susceptible to mechanical breakdown under dynamic loading, making it an ideal candidate for short-duration milling cycles where rapid fragmentation is desired.

Conversely, PLA filament exhibited a more gradual decline in surface area throughout the 60-minute milling period. The material retained over 42% of its original surface area even after prolonged milling, highlighting its inherent resistance to fast mechanical degradation. This behavior is likely due to PLA's fibrous and brittle polymeric structure, which does not lend itself easily to pulverization. Instead of breaking into small particles upon impact, PLA tends to shred into elongated segments. Furthermore, the mechanical strength provided by its polymer chains increases its resistance to compression and shear forces, thereby reducing the overall efficiency of the milling process under current system conditions.

Steel chips demonstrated a mixed behavior pattern. Initially, they showed only minimal reduction in surface area, indicating significant resistance to mechanical fragmentation—consistent with their high hardness and toughness. However, after extended exposure to milling forces, the material began to break down more significantly. By the end of the 60-minute process, steel chips had lost over 67% of their surface area. This gradual response suggests that prolonged milling is effective in reducing the size of tough metallic materials,

although it requires a higher energy input over an extended period.

While the system functioned effectively for the purpose of comparative evaluation, the experimental setup offers several opportunities for improvement. One limitation encountered was the insufficient impact energy delivered to PLA samples, which could not be milled efficiently under the current ball-to-powder ratio. The system was deliberately operated below the commonly recommended 30% drum fill volume due to mechanical load constraints. The total weight exerted on the system was calculated to be approximately 13.7 kN, which approaches the dynamic load limit of the selected bearings rated at 14.03 kN. To avoid operational risks, the fill volume was kept at a reduced level. Future iterations of this design could involve the use of higher capacity bearings or structurally reinforced components to allow for operation at optimal ball load levels, thereby enhancing the grinding effectiveness for more resistant materials.

Moreover, the current system operates with a constant motor speed. Implementing a variable-speed motor would provide better adaptability for different material types, enabling lower speeds for brittle metals and higher speeds for polymeric or ductile materials. This flexibility could allow the system to maintain optimal energy transfer rates across a broader range of experimental conditions. Additionally, long-duration milling was observed to result in elevated internal temperatures, which may pose a risk for thermally sensitive materials such as PLA. Incorporating an active cooling mechanism or airflow ventilation system may help to stabilize internal conditions and prevent heat-induced degradation.

The internal geometry of the drum could also be modified to enhance particle movement and reduce dead zones where materials accumulate without effective contact. Surface modifications or internal fins could promote more uniform circulation and ensure a consistent collision profile between grinding media and target material. These geometric enhancements would be particularly beneficial in achieving finer particle sizes and more efficient fragmentation in shorter time intervals.

Finally, expanding the experimental protocol to include multi-stage milling or material-specific parameter adjustments would allow a more comprehensive understanding of each material’s unique fragmentation behavior. For instance, an initial coarse grinding stage followed by a fine milling phase could optimize performance for harder materials like steel, while polymers might benefit from higher energy collisions over shorter durations.

In conclusion, although the system achieved its primary objective of comparing material-specific grinding efficiency, several key improvements could enhance its versatility and

effectiveness in future applications. These include structural reinforcements for higher load capacities, implementation of dynamic speed control, thermal regulation systems, and internal drum geometry optimizations. Such modifications would enable more efficient operation across a wider variety of materials, especially when working with heterogeneous combinations of metals and polymers.

6. Conclusion

In this study, a previously idle centrifugal casting machine was successfully redesigned and transformed into a functional ball milling system. The modification process included mechanical redesigns, such as a two-part drum cover for safety, as well as electrical upgrades, including a star-wired motor connection for better protection. Structural and load-based analysis enabled the selection of suitable support bearings and ensured mechanical stability during operation.

After completing the design, an experimental setup was established to evaluate the grinding performance of three different materials: SD52 steel chips, PLA filament, and aluminum foil. Each material was milled for one hour, and samples were collected every 15 minutes for surface area measurement. The results showed that grinding behavior significantly depends on the physical and mechanical characteristics of each material. Aluminum foil responded rapidly but with some inconsistency, steel required extended milling time due to its hardness, and PLA showed a stable and gradual breakdown.

The outcomes demonstrate that the redesigned machine is effective, economical, and capable of processing various materials with satisfactory results. This transformation proves that with the right engineering approach, existing equipment can be repurposed to serve new manufacturing functions. Future improvements may include using variable speed control, sealed enclosures for better dust management, or automated sampling for more detailed analysis.

REFERENCES

[1] A. &. Y. D. S. Gupta, Mineral Processing Design and Operation, Amsterdam: Elsevier, 2006.

[2] C. Suryanarayana, Mechanical alloying and milling. Progress in Materials Science, 2001, pp. 1-184.

[3] C. C. Koch, Structural nanocrystalline materials: an overview. Journal of Materials Science, 2007, p. 1403–1414.

[4] «https://commons.wikimedia.org/wiki/File:Svorkovnice_asynchronniho_motoru_do_hvezdy_a_do_trojuhelnika.svg,».

[5] «https://www.rulmansepetim.com/urun/ucp-205-skf-yatakli-rulman-ic-cap-25mm,».

APPENDICES

Table 7 Experiment Samples of the Aluminum Foil

0	15	30	45	60
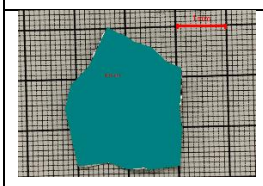		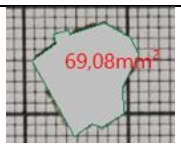		
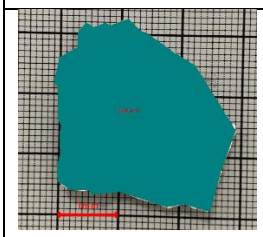	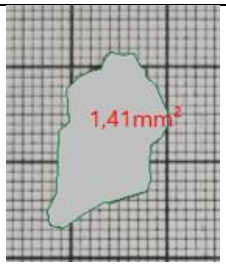	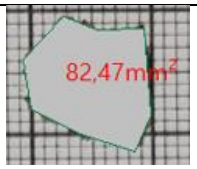		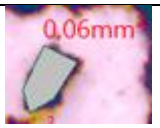
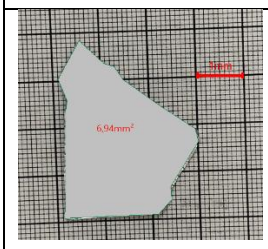	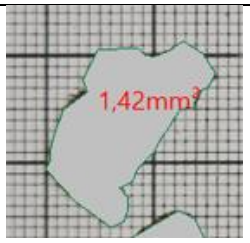	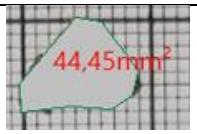		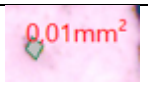
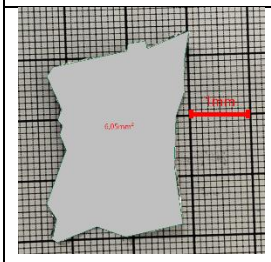	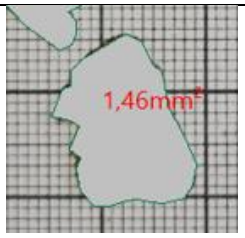	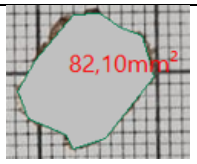		
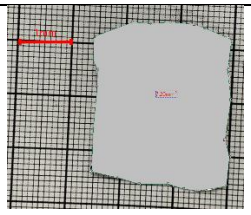	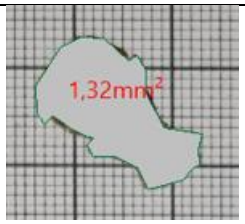	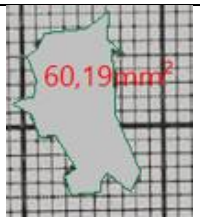		
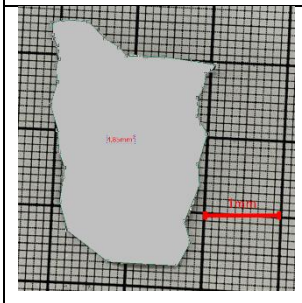	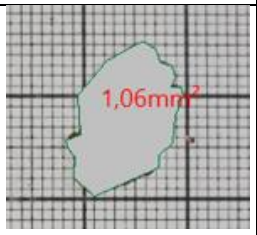			

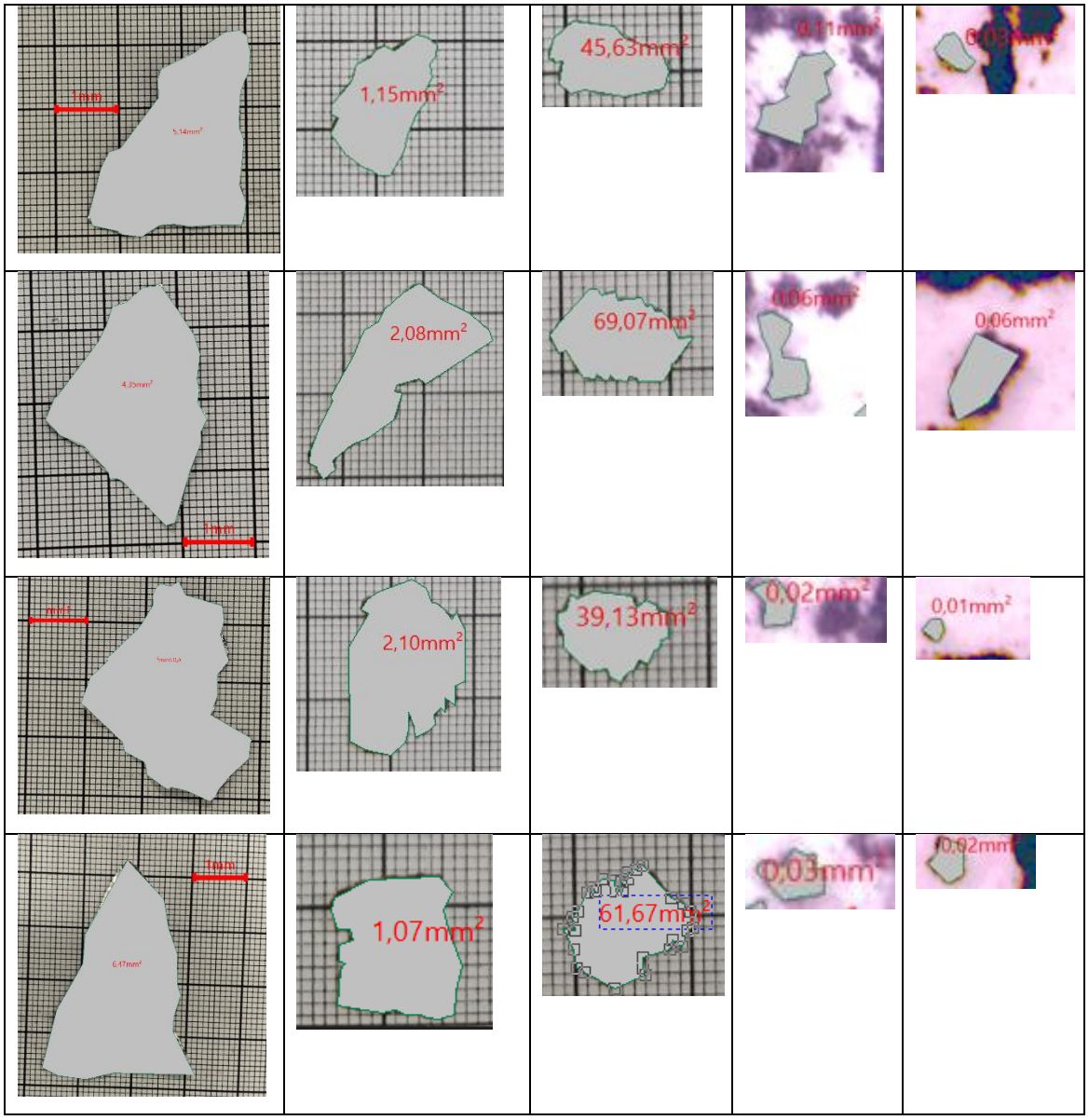

Table 8 Experiment Samples of the Steel Chips

0	15	30	45	60
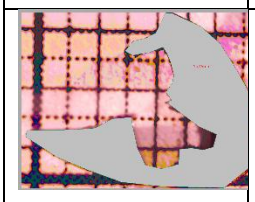	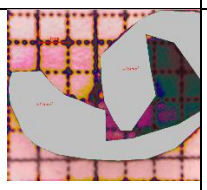	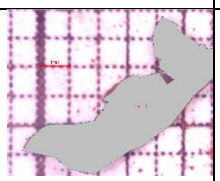	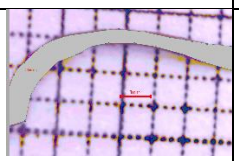	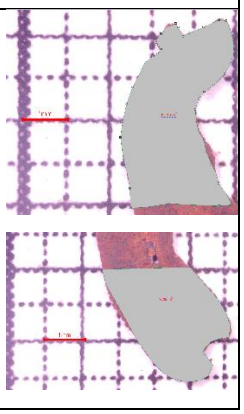

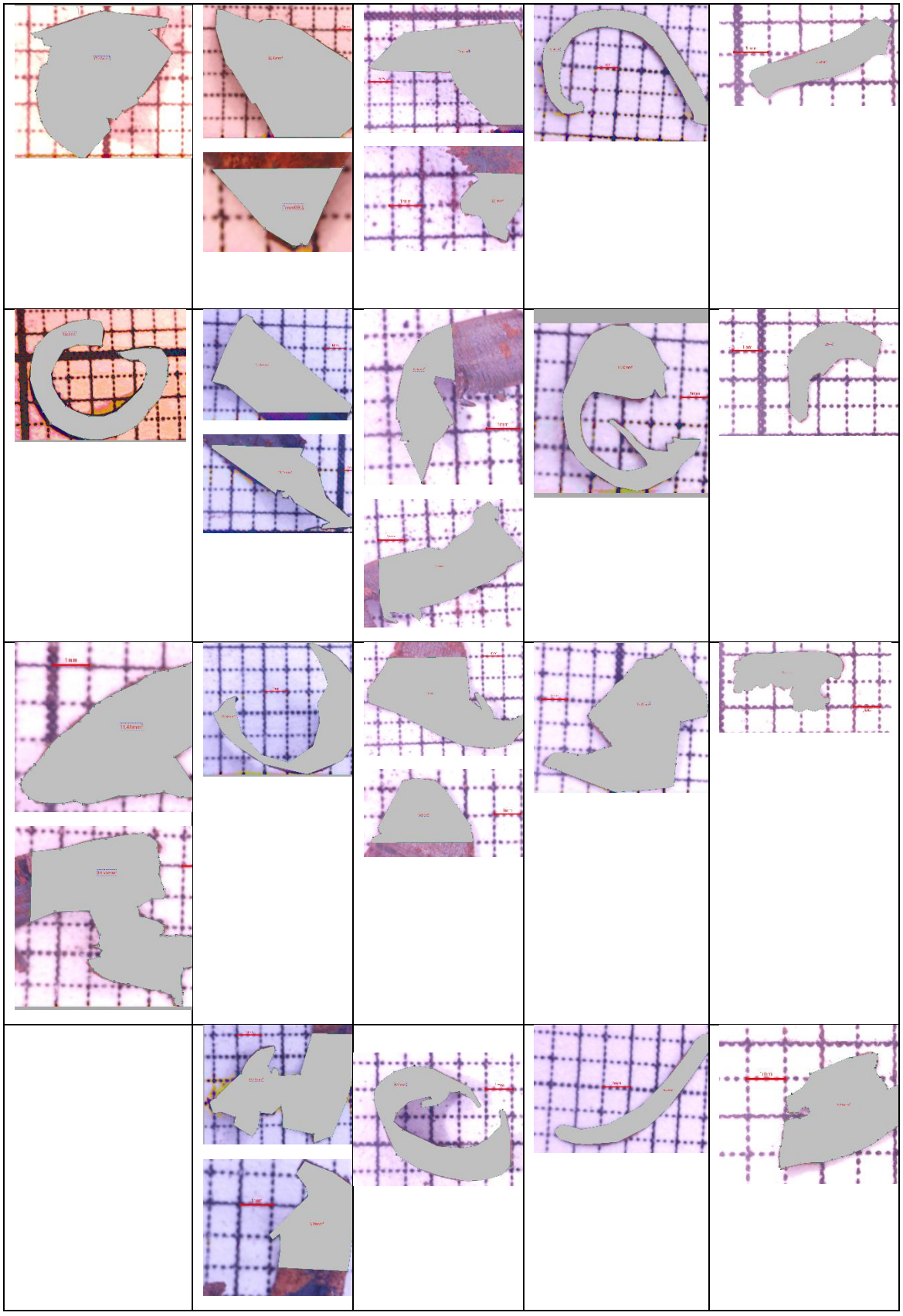

	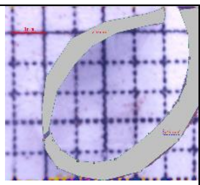	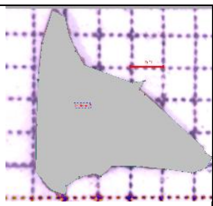	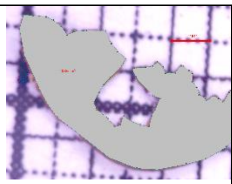	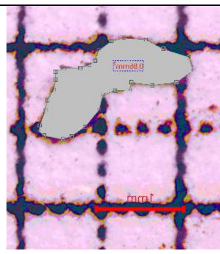
	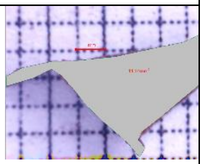	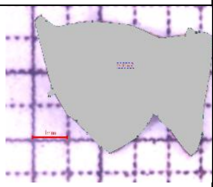	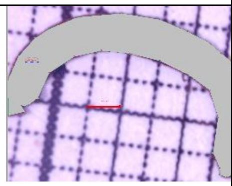	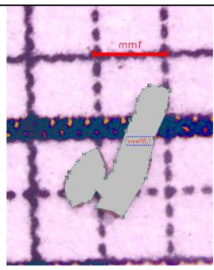
	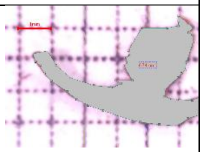	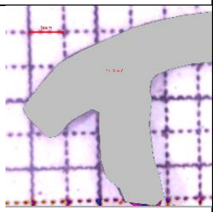	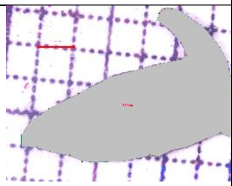	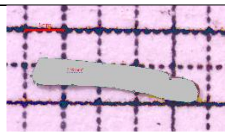
	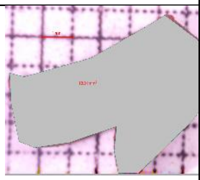	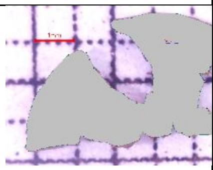	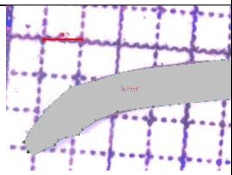 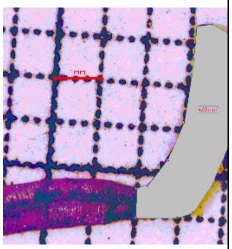	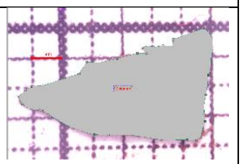
	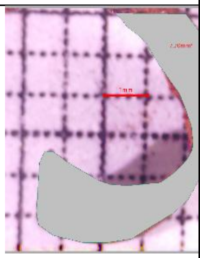	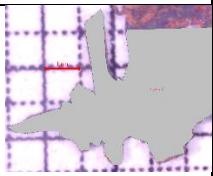 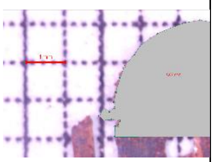	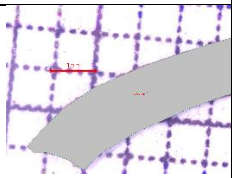	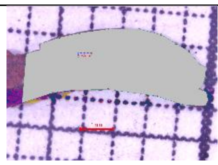 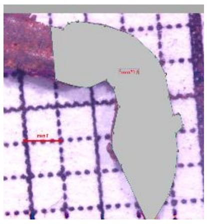

Table 9 Experiment Samples of the PLA Filament

0	15	30	45	60
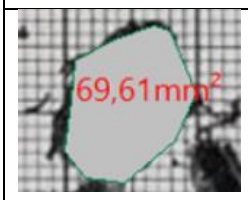	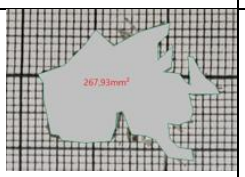	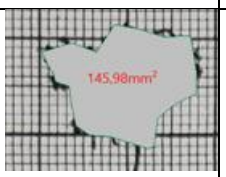		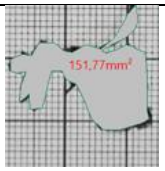
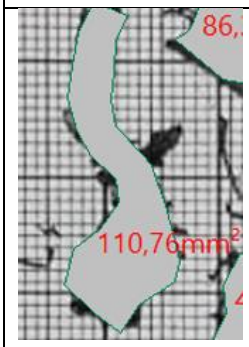	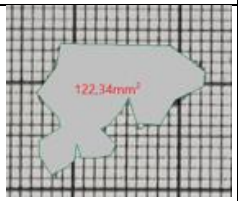	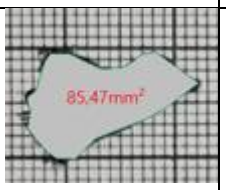		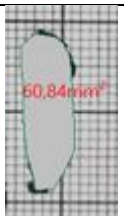
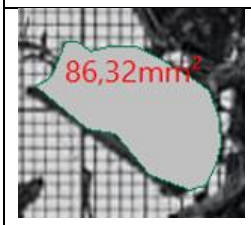	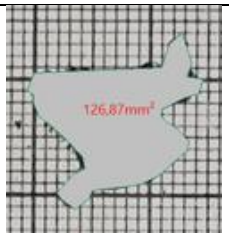	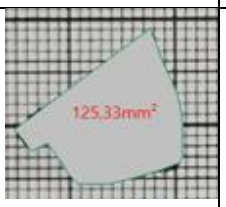		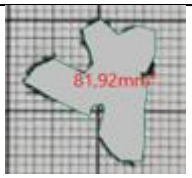
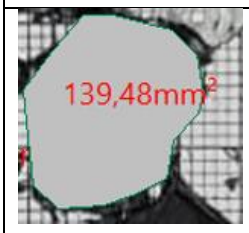	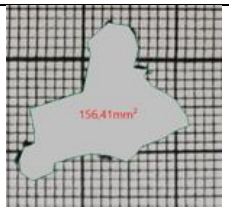	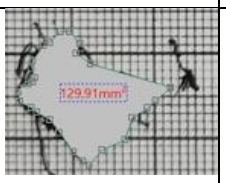	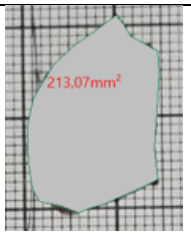	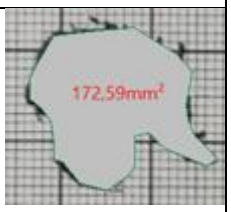
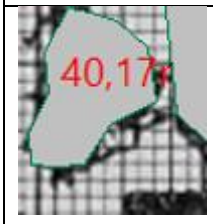	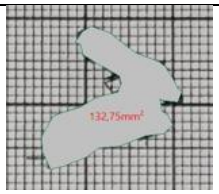	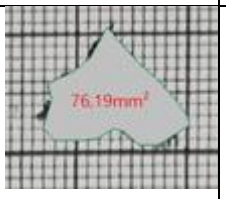	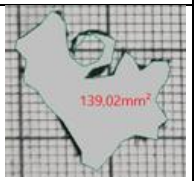	
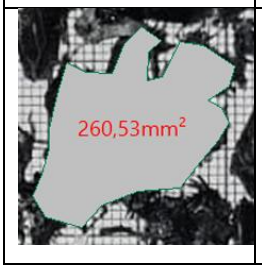	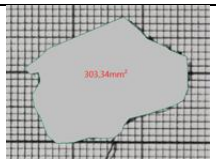	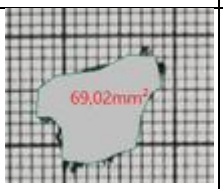	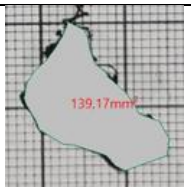	

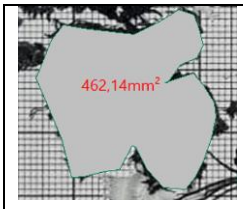 462,14mm²	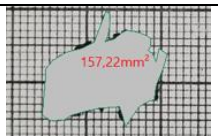 157,22mm²	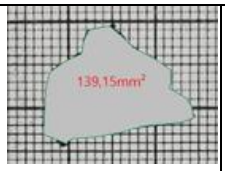 139,15mm²	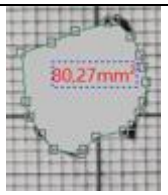 80,27mm²	 64,63mm²
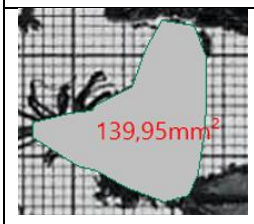 139,95mm²	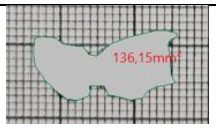 136,15mm²	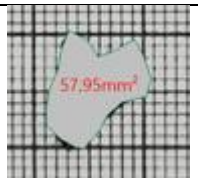 57,95mm²	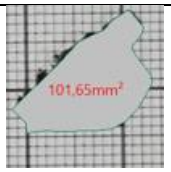 101,65mm²	 125,06mm²
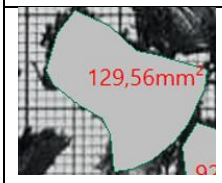 129,56mm²	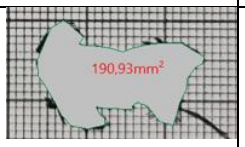 190,93mm²	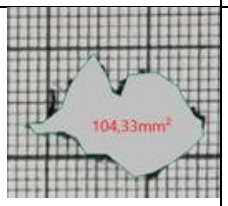 104,33mm²	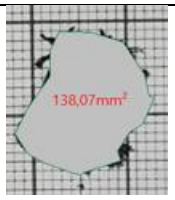 138,07mm²	 47,22mm²
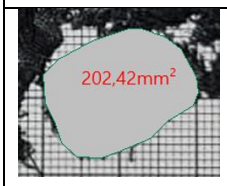 202,42mm²	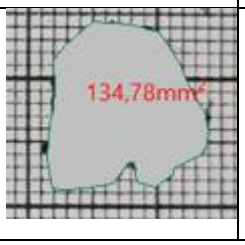 134,78mm²	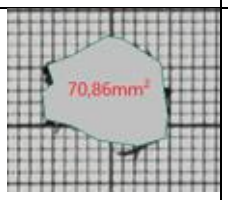 70,86mm²	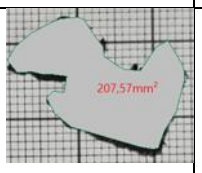 207,57mm²	 39,72mm²